Dissociation dynamics in the dissociative electron attachment to carbon dioxide

Pamir Nag and Dhananjay Nandi*
Indian Institute of Science Education and Research (IISER) Kolkata, Mohanpur 741246, India
(Received 2 March 2015; published 12 May 2015)

Dissociative electron attachment (DEA) to gas phase CO_2 has been probed using a velocity slice imaging technique. DEA to CO_2 produces only an O^- ionic fragment and shows two major resonances located at 4.4 and 8.2 eV, respectively. The kinetic energy and angular distribution of the O^- ions are measured around the second resonance with higher efficiency and sensitivity that provide details of the DEA dynamics. The kinetic energy distributions are in good agreement with the previous reports. However, the distinct angular distributions show substantial difference from the two recent studies within the limited electron energies. Our angular distribution results show two negative ion resonant states are involved in the underlying DEA process at the entire electron energies over the second resonance. We discussed the recent conflicting findings in the angular distribution results. The forward-backward asymmetry observed in the angular distributions is explained due to the interference effect of different partial waves associated with the attaching electron.

DOI: 10.1103/PhysRevA.91.052705 PACS number(s): 34.80.Ht, 34.80.Gs

I. INTRODUCTION

Carbon dioxide (CO_2) is an important atmospheric component and plays a significant role in gaseous electronic applications like CO_2 lasers. The low-energy vibrational cross section curves show several interesting features that pose some challenging theoretical questions [1]. CO_2 is isoelectronic with N_2O and both are linear in their ground states. It has been shown that these two molecules have similar total cross sections for both electron and positron scattering [2] measurements. Electron scattering experiments [3] have shown very good agreement between the differential cross sections for N_2O and CO_2 for higher incident electron energies. Electron scattering from CO_2 and dissociative electron attachment (DEA) to CO_2 continue to attract the attention of both theorists and experimentalists owing to the fact that the linear ground state becomes considerably bent when an electron attaches forming CO_2^-. DEA in CO_2 leading to the formation of only O^- ions has been studied extensively using a variety of techniques in the past four decades and has been reviewed by Chantry [4]. Those initial studies mainly focused on cross section and kinetic energy distribution measurements; no angular distribution measurements were attempted till the recent past.

DEA to CO_2 is a unique system to explore in the gas phase as it produces only O^- *via* two pronounced resonances at 4.4 and 8.2 eV, with the second resonance dominating. DEA is a two step process and can be written as

$$CO_2(X\,^1\Sigma_g{}^+) + e^- \rightarrow CO_2^{-*} \rightarrow O^- + CO \qquad (1)$$

with a threshold energy of 3.99 eV. This value is calculated from the established thermochemical data [5]: bond dissociation energy, $D(OC-O) = 5.45$ eV, and electron affinity, $A_e(O) = 1.46$ eV.

The kinetic energy of O^- ions produced from DEA to CO_2 was measured by Schulz [6] using the retarding field method and Schulz found that the ions are formed with very little kinetic energy and concluded that this was either due to the excess energy being deposited as vibrational energy of the CO fragment or to the negative ions being scattered primarily in the forward direction. The O^- kinetic energy distributions were also measured by Chantry [4] using a Wien filter. At the 8.2-eV resonance, the distribution had a broad peak at 0.6 eV in addition to a sharp peak close to 0 eV. Almost similar observations have been reported recently by Slaughter *et al.* [7] using a momentum imaging technique. However, the magnitude of the zero-energy peak is smaller and the 0.6-eV peak is even broader than that obtained by Chantry [4]. In any case, the observed low O^- kinetic energy indicates that most of the excess available energy is appearing as the internal (mainly vibrational) energy of CO.

Based on initial theoretical calculations [8,9] of the negative ion states of CO_2, the 8.2-eV resonance was assigned to a $^2\Sigma_g{}^+$ shape resonance (valence state). However, its calculated position in the Franck-Condon region does not agree with the measurements. Previous experimental observations [10–12] have suggested a mixed valence-Rydberg state (Π_g) supported by earlier *ab initio* calculations [9]. Very recently, both the kinetic energy and the angular distributions of the O^- ions from DEA to CO_2 have been measured at 8.2-eV [13–15] resonant energy and at 0.5 eV on either side [14,15] of the resonant energy (i.e., 7.7 and 8.7 eV) using a momentum spectroscopic or imaging technique. The kinetic energy distributions showed two peaks situated at 0 eV and at around 0.6 eV and more or less agreed with each other. However, the reported angular distribution data are very different from each other. Based on the measurements at three different electron energies in the range of 7.7–8.7 eV, Moradmand *et al.* [15] observed that the angular distributions peaked at 45° and 135° with little forward-backward asymmetry. They also observed that the angular distributions did not depend on the primary electron energy in the range of study, which is contradictory to the results reported by Wu *et al.* [14] in which the distribution varied significantly with the primary energy. The observed results were attributed to the $^2\Pi_g$ Feshbach resonant state of CO_2^-. However, they could not exclude the possibility of different closely lying states involved in the DEA process.

In this context, we report detailed systematic studies of DEA to CO_2 around the 8.2-eV resonance using a velocity slice imaging (VSI) technique optimized for low-energy

*dhananjay@iiserkol.ac.in

electron-collision experiments. Here, we report distinct kinetic energy and angular distributions of the fragment ions. Our kinetic energy distribution data of the fragment ions more or less agree with all the previous reports; however, the angular distribution data have shown some interesting features that are discussed and highlighted in this paper.

II. EXPERIMENT

The present experiments were carried out using a highly differential momentum imaging technique. The experimental setup and technique are very similar to what has been reported [16] earlier. In brief, the setup consists of a home-built pulsed electron gun with a typical energy resolution of 0.6 eV, a Faraday cup to measure the electron current, and a velocity map imaging (VMI) spectrometer to measure the momentum distribution. The measurements are performed under an oil-free high-vacuum condition at a base pressure of below $\sim 10^{-9}$ mbar. A magnetically well-collimated pulsed electron beam of 200 ns in duration, 10 kHz in repetition, and of controlled energy is passed through the interaction region where it interacts with an effusive molecular beam produced by a capillary tube. The negative ions are formed under low-energy electron capture with the isolated molecules. The molecular beam is directed towards the detector and along the axis of the spectrometer. The magnetic field used to collimate the electron beam is about 40 G. A pair of magnetic coils (Helmholtz type) is mounted outside the vacuum chamber to produce a uniform magnetic field at the region of interaction. After the electron beam has passed, a moderate pulsed extraction field is applied and the negative ions are extracted from the source region into the VMI spectrometer. The extraction pulse duration used in the present measurement is about 900 ns and is applied 200 ns after the electron beam has passed. The delayed extraction provides an appropriate time spread for better time slicing.

The VMI spectrometer is like a three-field time-of-flight spectrometer which focuses ions starting from a finite volume onto a two-dimensional position-sensitive detector such that ions of a given velocity are mapped to one point on the detector irrespective of their spatial location in the source region. The time of flight (ToF) of the detected ions is determined using the signal taken from the back side of microchannel plate (MCP) assemble whereas the x and y positions of each detected ion are calculated from the position decoding anode [17]. The (x,y) position along with the ToF of each detected particle is acquired and stored in list-mode format (LMF). The central slice of the "Newton sphere" contains the full angular and translational energy information. The central time-slice image is obtained by selecting the appropriate time window during offline analysis of the LMF file. This time-slice image corresponds to the ions ejected in the plane parallel to the detector containing the electron beam axis.

III. EXPERIMENTAL RESULTS

Figure 1 shows the ion yield curve as a function of electron energy for the formation of O^- from DEA to a CO_2 molecule. The curve shows two well-separated resonances located around 4.4 and 8.2 eV, in good agreement with earlier reports [4,18]. From the previous studies it was suggested that the lower peak is associated with the $^2\Pi_u$ shape resonance and

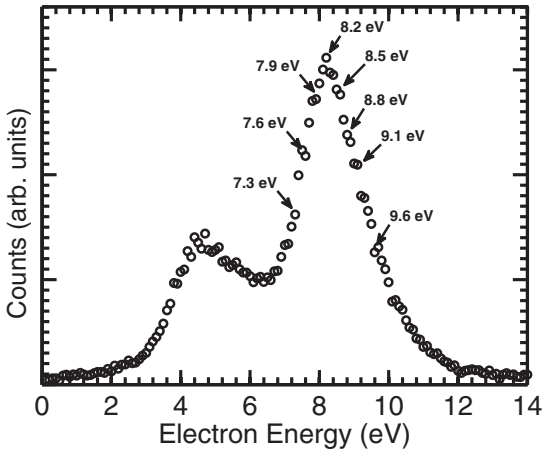

FIG. 1. The ion yield curve of O^- arising from DEA to CO_2 as a function of electron energy. The arrows indicate the energies at which the velocity slice images are taken.

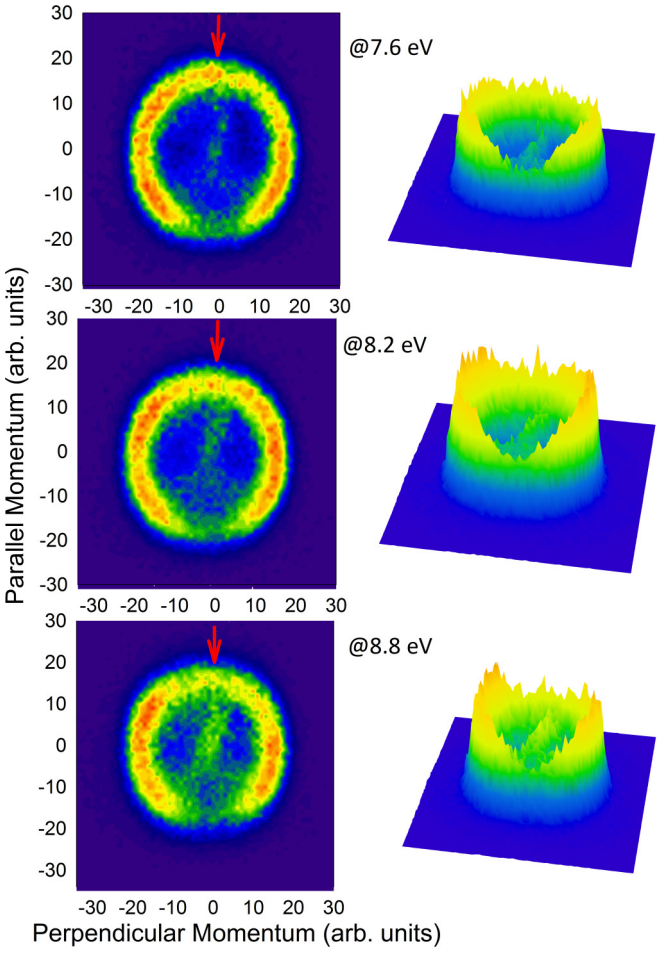

FIG. 2. (Color online) Velocity slice images of O^- ions taken at different electron energies around resonance as indicated. The left panel shows the two-dimensional pattern after time slicing. The electron beam direction is vertically down. The right panel shows the corresponding three-dimensional distribution with intensity as the z axis.

that at higher energies it is associated with an electronically excited $^2\Pi_g$ Feshbach-type resonance [7]. The arrows indicate the electron energies at which the velocity slice images are taken. Figure 2 represents the VSIs taken at incident electron energies of 7.6, 8.2, and 8.8 eV for comparison with the images provided in Fig. 2 of Ref. [14]. The direction of the electron beam is from top to bottom as indicated by the arrows. The distributions show only one ring pattern with small distribution at the center of the images. The weak intensities of each of the images imply an ion kinetic energy of nearly 0 eV. Besides the weak intensities with low kinetic energy, broader distributions are also observed. The images do not show any noticeable change in either the diameter or the pattern as the electron energy changes around the resonance. The images clearly show forward-backward asymmetry in the angular distribution. In comparison with the reported images taken at 8.2 eV, our velocity slice image at the same energy is very similar to that of Slaughter *et al.* [7,13], but is significantly different from that of Wu *et al.* [14]. Such differences could be due to the implementation of different experimental techniques: we employed VMI, Slaughter *et al.* [7] used a COLTRIMS-type spectrometer for momentum imaging, and Wu *et al.* implemented both spatial and velocity focusing. Furthermore, Wu *et al.* additionally used wire mesh in the path of the ion trajectory, which can significantly affect the imaging technique [19].

IV. DISCUSSIONS

In this section we present a detailed analysis of the VSIs in order to obtain the kinetic energy and angular distributions from the images.

A. Kinetic energy distributions

The kinetic energy distributions normalized with the O^- counts at the 0.4-eV peak position arising from the DEA to CO_2 around the 8.2-eV resonance are shown in Fig. 3.

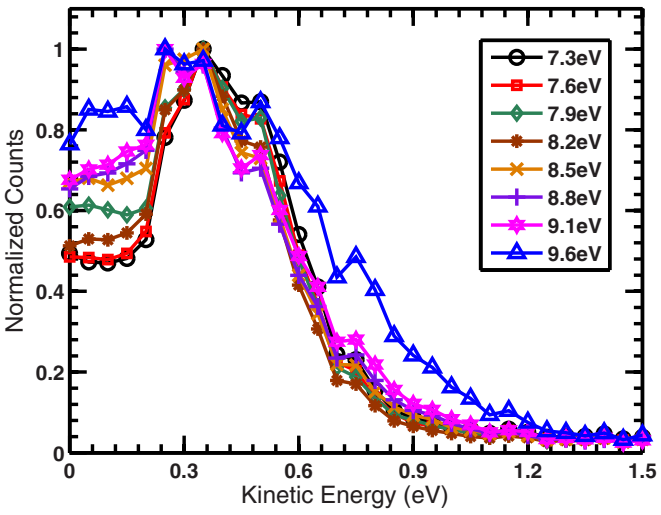

FIG. 3. (Color online) Kinetic energy distributions of O^- from DEA to CO_2 at different incident electron energies around the 8.2-eV resonance. The distributions shown are obtained after integrating over entire 2π angles about the electron beam direction and normalized at the 0.4-eV peak.

The kinetic energy distributions are obtained by integrating over the entire ejection angle of the O^- fragment and plotting them as a function of the kinetic energy. The present kinetic energy distribution of the ions shows two kinetic energy values at nearly 0 eV and around 0.4 eV that are very consistent with the all earlier reports [14,15] except that the distribution is narrower in our cases. The observed broadening in the distributions for different studies could be due to mainly two reasons: (i) different energy resolution of the incident electron beam and (ii) different slice width used in different experiments as thoroughly discussed by Adaniya *et al.* [20]. For example, the typical energy resolution of our electron gun is 0.6 eV, whereas it is about 1 eV for the electron gun used by Moradmand *et al.* [15]. The typical full width at half maximum (FWHM) of the ToF of O^- ions produced in this energy range is about 300 ns and we have taken a 50-ns thin slice from the central part of the Newton sphere. A theoretical attempt [21] had been made previously to understand the two-peak structure observed [4] in the kinetic energy distribution using the potential energy surface of $CO_2^-(^2\Sigma_g{}^+)$. However, recent studies [10,11,14] suggest that a $^2\Sigma_g{}^+$ state is not responsible for the 8.2-eV resonance, but rather a doubly excited $^2\Pi_g$ Feshbach resonant state of CO_2. Assuming the dissociation is a two-body breakup that is true for this energy and considering the conservation of energy, one can determine the kinetic energy distribution and internal energy of the neutral fragment (i.e., CO). The threshold for O^- formation from the electron attachment to CO_2 is 4.0 eV, which leaves about 4.2 eV excess energy that is distributed amongst the fragment's translational and internal energy. The small kinetic energy peak at nearly 0 eV implies that the neutral fragment, CO, is left in a vibrational (v) and/or rotational (j) excited state. The main peak in the distribution implies that the neutral fragment will be populated to a vibrational level ($v' < v$) and/or a rotational level of CO lower than that of the previous case. More importantly, the most probable kinetic energy remains unchanged as the initial electron energy increases. However, as clearly seen from the kinetic energy distribution (Fig. 3), the number of low-energy ions increases as the electron energy increases. Thus, it is quite obvious that a large fraction of the initial energy is deposited in the CO fragment and this fraction increases as the incident energy increases. This strongly suggests that the O^- ions are created with low kinetic energy leaving the CO fragment in an enormous rovibrationally excited state, which may lead to the dissociation process even faster. A time-resolved nuclear dynamics measurement could quantify the above claim.

As already described, DEA is a two-step process. In the first step, the electron gets captured by the molecule forming the temporary negative ion (TNI) state, and in the second step, the TNI dissociates into a fragment negative ion(s) and neutral fragment(s). After TNI formation, the molecular configuration changes from linear to bending geometry. However, the TNI does not undergo any considerable rotation before the dissociation takes place. Under these assumptions, the symmetries of the resonant states involved in the process could be adequately described by the detailed angular distributions (differential cross sections) of fragment negative ions, which are analyzed and presented below.

B. Angular distributions

The symmetry of the resonant state(s) involved can be revealed from the analysis of angular distributions of the fragment ions. As shown, DEA to CO_2 produces only O^- ions and the studied resonance energy is below the ionization energy; the dissociation behavior can be treated like that of a diatomic molecule. A generic expression for the angular distribution of a fragment ion from a diatomic molecule has been given by O'Malley and Taylor [22] as

$$f(k,\theta,\phi) \sim \sum_{|\mu|} \left| \sum_{l=|\mu|}^{\infty} a_{l\mu}(k) Y_{l\mu}(\theta,\phi) \right|^2, \qquad (2)$$

where k is the incident electron momentum, $a_{l\mu}(k)$ are energy-dependent expansion coefficients, $Y_{l\mu}(\theta,\phi)$ are the spherical harmonics, μ is the difference in the projection of the angular momentum along the internuclear axis for the neutral molecular state and the negative ion resonance state, given as $\mu = |\Lambda_f - \Lambda_i|$, and l is the angular momentum of the incoming electron with values given by $l \geqslant |\mu|$. Notice that the extra electron carries one-half unit of spin; thus the inherent spin selection rule follows in DEA. To correlate with the experimentally observed angular distribution, one wants the dependence of the cross section on the angle θ between the direction of dissociation and k_i. With the same assumption, Azria *et al.* [23] have adopted a similar treatment for polyatomic molecules and found the following expression for the angular distribution in the laboratory frame by averaging over the angle ϕ:

$$f(\theta) \propto \frac{1}{2\pi} \int_0^{2\pi} \left| \sum_{l,m,\epsilon} i^l \exp(i\delta_l) a_{lm}^{\epsilon} X_{lm}^{\epsilon *}(\theta,\phi) \right|^2 d\phi, \qquad (3)$$

where (θ,ϕ) are the polar angles of k_i in the dissociation frame (in which the z axis has the direction of the bond that breaks). For attachment involving a given resonance, the expected angular distribution is a combination of the partial distributions for each allowed value of l. However, the general shape is given by a linear combination of these partial distributions with coefficients $(a_{lm}^{\epsilon})^2$.

Considering the above formalism, we have fitted the measured angular distribution of the ions using the equation

$$f(\theta) = \sum_{|\mu|} \left| \sum_{j=|\mu|} a_j e^{i\delta_j} Y_{j\mu} \right|^2, \qquad (4)$$

where the summation over μ is due to the involvement of different states in the process. As mentioned earlier, the ground state of neutral CO_2 is the $^1\Sigma_g{}^+$ ($\Lambda_i = 0$) state; thus the values $\mu = 0$, 1, and 2 correspond to the transitions to Σ, Π, and Δ, respectively. a_j's are the relative weighting factors of the different partial waves and δ_j's denote the phase differences of each of the partial waves with respect to the lowest-order partial wave responsible for the particular transition.

The experimentally observed angular distributions taken at the indicated electron energies around the second resonance are shown in Fig. 4. Angular distributions clearly show no initial energy dependence up to 8.8 eV and a strong energy dependence above 8.8 eV has been observed. Our observations

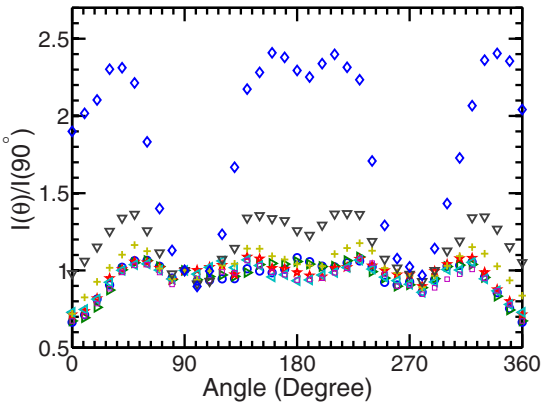

FIG. 4. (Color online) Angular distributions of the O^- ions arising from DEA to CO_2 for the indicated electron energies around the second resonance. The distributions shown here are for (○) 7.3 eV, (▷) 7.6 eV, (★) 7.9 eV, (◁) 8.2 eV, (□) 8.5 eV, (+) 8.8 eV, (▽) 9.1 eV, and (◇) 9.6 eV incident electron energies.

confirm recent reports [7,15] using imaging techniques, but are significantly different from those of Wu *et al.* [14] in their energy range of study. The recent studies reported the O^- angular distribution at the same three electron energies around the resonance, namely, 7.7, 8.2, and 8.7 eV. The two results contradict each other. Moradmand *et al.* [15] did not observe any energy dependence in their angular distribution data, whereas Wu *et al.* [14] observed a strong energy dependence in their data within the limited energy range studied. We observed a strong energy dependence at a higher energy than reported.

From their experimental findings, Moradmand *et al.* [15] concluded the involvement of only one $^2\Pi$ Feshbach resonant state in the DEA process at the 8.2-eV resonance. In another study by combining experimental results and an *ab initio* theoretical approach, Slaughter *et al.* [7] showed that the 8.2-eV resonance is initiated by electron attachment to a dissociative, doubly excited $^2\Pi_g$ state that interacts with a lower $^2\Pi_u$ shape resonance through a conical intersection and dissociates to electronic ground state products. The authors also employed theory to determine the entrance amplitude in the ions' angular distribution for the axial recoil approximation and suggested a departure from the approximation. On the other hand, Wu *et al.* [14] could explain their experimental results within the axial recoil approximation and involving one $^2\Pi$ resonant state at two higher energies (8.2 and 8.7 eV) studied. However, for the lower energy (7.7 eV) the results were discussed using Σ and Δ parities that were generated from the state splitting in the near-zone of the $^2\Pi_g$ resonance state due to the Renner-Teller (RT) effect. The significant backward scattering pattern observed by Wu *et al.* at 7.7 eV was also explained in light of the RT effect leading to the state splitting in the near-zone $^2\Pi_g$ resonance. In the following paragraph we show that two negative ionic states are required to satisfactorily explain our observed data and we also observed that the dominating state is a Σ symmetry instead of a Π symmetry with minor contributions coming from an additional Δ state at lower energies and a Π state at higher energies.

TABLE I. The fit parameters for the O^- angular distribution at various lower electron energies with contributions from both Σ and Δ states. The a_j's and c_l's are the relative strengths of various partial waves for the Σ and Δ states, respectively. The δ_m's (in rad) are the relative phases of each partial wave with respect to the lowest-order partial wave responsible for the particular transition (please see the text).

	7.3 eV	7.6 eV	7.9 eV
Weighting ratio of different partial waves			
a_0:a_1:a_2:a_3	1:4.61:1.28:1.04	1:0.49:0.08:0.16	1:8.16:1.57:1.94
c_2:c_3:c_4:c_5	3.67:1.96:1.29:0.29	0.25:0.10:0.14:0.01	7.25:1.03:1.49:1.05
Phase difference (Σ)			
δ_{s-p},δ_{s-d},δ_{s-f} (rad)	0.18, 2.15, 3.87	1.64, 1.76, 4.33	0.81, 5.34, 3.52
Phase difference (Δ)			
δ_{d-f},δ_{d-g},δ_{d-h} (rad)	1.86, 4.01, 0	4.53, 2.73, 0.01	2.60, 2.22, 4.50

TABLE II. The fit parameters for the O^- angular distribution at 8.2-eV electron energy with contributions from both $\Sigma + \Delta$ (left side) and $\Sigma + \Pi$ (right side) final states. The a_j's, b_k's, and c_l's are the relative strengths of various partial waves for the Σ, Π, and Δ states, respectively. The δ_m's (in rad) are the relative phases of each partial wave with respect to the lowest-order partial wave responsible for a particular transition (please see the text).

	8.2 eV		8.2 eV
Weighting ratio		Weighting ratio	
a_0:a_1:a_2:a_3	1:3.98:0.51:0.65	a_0:a_1:a_2:a_3	1:0.54:0.95:0.77
c_2:c_3:c_4:c_5	3.63:0.74:0.51:0.20	b_1:b_2:b_3:b_4	1.03:2.33:0.92:0.02
Phase difference (Σ)		Phase difference (Σ)	
δ_{s-p},δ_{s-d},δ_{s-f} (rad)	0.82, 3.50, 4.03	δ_{s-p},δ_{s-d},δ_{s-f} (rad)	0.71, 3.15, 1.70
Phase difference (Δ)		Phase difference (Π)	
δ_{d-f},δ_{d-g},δ_{d-h} (rad)	2.88, 4.26, 1.66	δ_{p-d},δ_{p-f},δ_{p-g} (rad)	4.49, 3.02, 0.49

TABLE III. The fit parameters for the O^- angular distribution at various higher electron energies with contributions from the Σ final state only. The a_j's are the relative strengths of various partial waves for the Σ state. The δ_m's (in rad) are the relative phases of each partial wave with respect to the lowest-order partial wave responsible for the particular transition (please see the text).

	8.5 eV	8.8 eV	9.1 eV	9.6 eV
Weighting ratio of different partial waves				
a_0:a_1:a_2:a_3	1:0.45:0.09:0.11	1:0.49:0.09:0.12	1:0.67:0.07:0.10	1:1.14:0.12:0.13
Phase difference (Σ)				
δ_{s-p},δ_{s-d},δ_{s-f} (rad)	1.68, 2.20, 4.38	1.65, 2.14, 4.38	1.59, 3.07, 4.47	1.55, 3.39, 4.66

TABLE IV. The fit parameters for the O^- angular distribution at various lower electron energies with the contributions from both Σ and Π states. The a_j's and b_k's are the relative strengths of various partial waves for the Σ and Π states, respectively. The δ_m's (in rad) are the relative phases of each partial wave with respect to the lowest-order partial wave responsible for the particular transition (please see the text).

	8.5 eV	8.8 eV	9.1 eV	9.6 eV
Weighting ratio of different partial waves				
a_0:a_1:a_2a_3	1:0.67:0.38:0.50	1:6.84:1.71:7.73	1:0.55:0.50:0.59	1:0.29:0.42:0.89
b_1:b_2:b_3b_4	1.38:0.58:0.60:0	4.28:4.58:9.10:0.03	2.03:0.36:0.80:0.01	2.13:0.28:1.17:0.04
Phase difference (Σ)				
δ_{s-p},δ_{s-d},δ_{s-f} (rad)	3.48, 1.17, 1.31	0.47, 3.93, 2.89	1.76, 1.55, 2.92	2.59, 1.02, 2.03
Phase difference (Π)				
δ_{p-d},δ_{p-f},δ_{p-g} (rad)	1.08, 1.59, 0.73	3.51, 2.24, 1.65	2.13, 0.94, 1.54	1.81, 0.86, 0.84

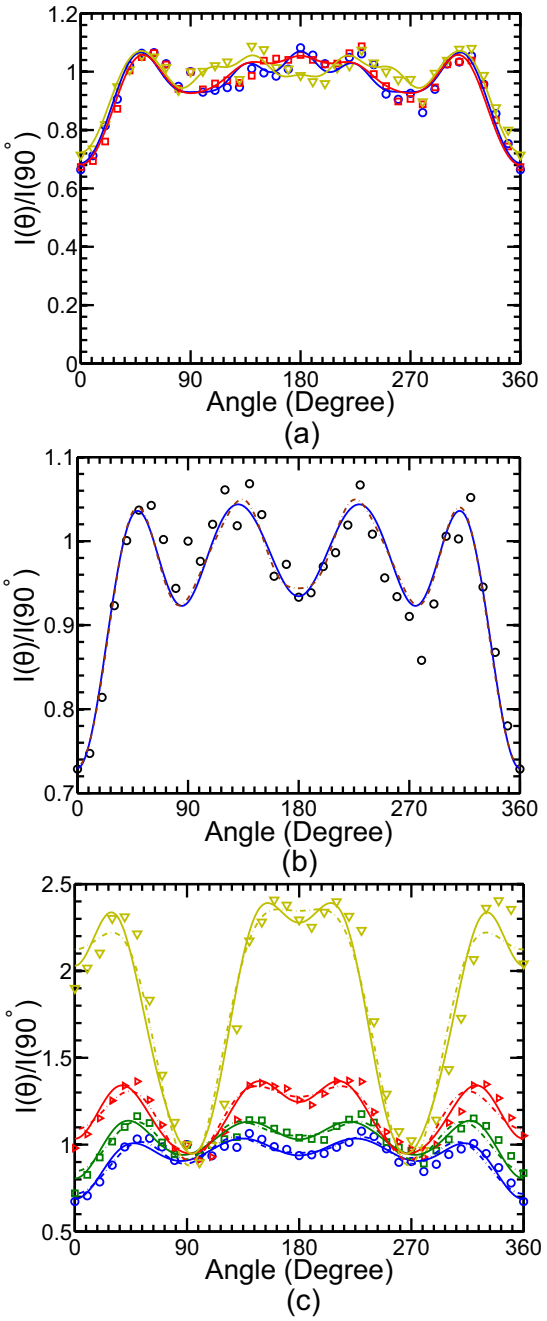

FIG. 5. (Color online) Fit to the angular distribution data of the O^- ions for the following incident electron energies around the resonance: (a) (○) 7.3, (□) 7.6, and (▽) 7.9 eV; (b) (○) 8.2 eV; and (c) (○) 8.5, (□) 8.8, (▷) 9.1, and (▽) 9.6 eV. The solid lines in panel (a) indicate the best fits obtained for the $\Sigma \rightarrow (\Sigma$ and $\Delta)$ final-state transitions. The dashed and solid lines in panel (b) indicate the best fits obtained for the $\Sigma \rightarrow (\Sigma$ and $\Delta)$ and $\Sigma \rightarrow (\Sigma$ and $\Pi)$ final-state transitions, respectively. The dashed and solid lines in panel (c) indicate the best fits obtained for the $\Sigma \rightarrow \Sigma$ only and $\Sigma \rightarrow (\Sigma$ and $\Pi)$ final-state transitions, respectively. The data have been fitted with Eq. (4) (see text for details).

As can be seen from Fig. 5 in order to get a satisfactory fit, we have to involve two negative ionic states with relatively large partial waves. In Fig. 5, we present the systematic studies of fit to the angular distribution data of the O^- ions for (a) the lower energies, (b) the resonance energy, and (c) the higher energies. The solid lines in Fig. 5(a) are the best fits obtained for the $\Sigma + \Delta$ final-state transition taking up to four partial waves for each state. The values of the fitted parameters (for the fit with R^2 in excess of 0.92) are listed in Table I. The dashed and solid lines in Fig. 5(b) are the best fits obtained for the $\Sigma + \Delta$ and $\Sigma + \Pi$ final-state transitions taking up to four partial waves for each state. The values of the fitted parameters (for the fit with R^2 in excess of 0.92) are listed in Table II. Finally, the dashed and solid lines in Fig. 5(c) are the best fits obtained for the Σ only and the $\Sigma + \Pi$ final-state transitions taking up to four partial waves for each state. The values of the fitted parameters (for the fit with R^2 in excess of 0.92) are listed in Table III for the first case and in Table IV. We used two final states throughout, only the Π final state did not give (R^2 is negative) us satisfactory fits; however, only the Σ final state gave reasonably good fits for higher energies as can be seen from Fig. 5(c). Note that we do not include explicitly the (u/g and +/-) symmetries of the TNI states used in the analysis.

Our observation could be explained from the computed potential energy curve of Claydon *et al.* [8]. As shown in Fig. 2 of Ref. [8], for linear geometry, a $^2\Sigma_g{}^+$ state is present in the Franck-Condon region around the resonant energy discussed here. Our findings could be more supportive if we consider the bending mode vibration as can be seen from Fig. 3 of Ref. [8]. The $^2\Sigma_g{}^+$ symmetry accessible from the Franck-Condon (FC) region is translated as an $^2A_1$ state and the $^2\Pi_u$ symmetry accessible from FC region splits into $^2B_1$ and $^2A_1$ states due to bent geometry [8]. The $^2B_1$ state is also responsible for this resonance as the $^2\Pi_u$ state observed from our angular distribution data as pointed out by Slaughter *et al.* [7]. The $^2A_1$ state could be responsible for the 4.4-eV resonance as discussed by Moradmand *et al.* [24].

The forward-backward asymmetry that we observed at the lower energy region is similar to that of Moradmand *et al.* [15] but is significantly different from that of Wu *et al.* [14]. As the electron energy increases the forward-backward asymmetry decreases; a similar observation has been found by Wu *et al.* However, we do not observe such behavior at the energy mentioned by Wu *et al.*, rather at a higher energy. As discussed above, the O^- production at the higher incident energies (above 8.8 eV) left the CO fragment in a vibrationally excited state. Our experimental results are well fit using this model. The change in the dynamics at 8.8 eV could be due to the onset of fast dissociation.

V. CONCLUSIONS

We have studied the detailed dynamics of DEA to CO_2 by measuring the DEA cross section, kinetic energy, and angular distribution of the only fragment negative ion produced in the process. Two major resonances have been observed in the cross section. The kinetic energy and angular distribution are studied around the second resonance. The kinetic energy distribution measurements show a significant amount of energy dissipated in the vibrational and/or rotational excitation of the neutral CO fragment. The distinct angular distributions over the resonance energy show no energy dependence at the lower energy and clearly show energy dependence at the higher energy.

The forward-backward asymmetry observed at the lower energy decreases as the electron energy increases. The angular distributions show that at least two negative ion resonance states are involved in the dynamics and also indicate the role of higher partial waves. The angular distributions also indicate the role of resonances of Σ and Π symmetry accessible from the Franck-Condon region. The $^2\Sigma_g{}^+$ symmetry translates into an $^2A_1$ state and $^2\Pi_u$ symmetry splits into $^2B_1$ and $^2A_1$ due to their bent geometry. In contrast to the previous studies where a single Π symmetry has been proposed, we observed that a single Σ symmetry could explain our results to a certain extent, with only Π symmetry giving a negative R^2 fit. The observed forward-backward asymmetry has been explained due to the interference between the different partial waves involved in the process. The change in the dynamics at 8.8-eV incident energy has been discussed due to the onset of fast dissociation. In order to really understand the underlying dynamics, a detailed theoretical calculation is strongly recommended.

ACKNOWLEDGMENTS

D. Nandi gratefully acknowledges financial support from the "Indian National Science Academy" for supporting this research under the INSA Young Scientist Project "SP/YSP/80/2013/734."

[1] M. Allan, J. Phys. B **35**, L387 (2002).
[2] C. K. Kwan, Y. F. Hsieh, W. E. Kauppila, S. J. Smith, T. S. Stein, M. N. Uddin, and M. S. Dababneh, Phys. Rev. Lett. **52**, 1417 (1984).
[3] W. M. Johnstone and W. R. Newell, J. Phys. B **26**, 129 (1993).
[4] P. J. Chantry, J. Chem. Phys. **57**, 3180 (1972).
[5] NIST Chemistry WebBook, http://webbook.nist.gov/.
[6] G. J. Schulz, Phys. Rev. **128**, 178 (1962).
[7] D. S. Slaughter, H. Adaniya, T. N. Rescigno, D. J. Haxton, A. E. Orel, C. W. McCurdy, and A. Belkacem, J. Phys. B **44**, 205203 (2011).
[8] C. R. Claydon, G. A. Segal, and H. S. Taylor, J. Chem. Phys. **52**, 3387 (1970).
[9] W. B. England, B. J. Rosenberg, P. J. Fortune, and A. C. Wahl, J. Chem. Phys. **65**, 684 (1976).
[10] M. A. Huels, L. Parenteau, P. Cloutier, and L. Sanche, J. Chem. Phys. **103**, 6775 (1995).
[11] S. K. Srivastava and O. J. Orient, Phys. Rev. A **27**, 1209 (1983).
[12] R. I. Hall, A. Chutjian, and S. Trajmar, J. Phys. B **6**, L264 (1973).
[13] D. Slaughter, H. Adaniya, T. Osipov, D. Haxton, T. Weber, T. Rescigno, B. McCurdy, and A. Belkacem, J. Phys.: Conf. Ser. **388**, 052013 (2012).
[14] B. Wu, L. Xia, Y.-F. Wang, H.-K. Li, X.-J. Zeng, and S. X. Tian, Phys. Rev. A **85**, 052709 (2012).
[15] A. Moradmand, D. S. Slaughter, A. L. Landers, and M. Fogle, Phys. Rev. A **88**, 022711 (2013).
[16] D. Nandi, V. S. Prabhudesai, E. Krishnakumar, and A. Chatterjee, Rev. Sci. Instrum. **76**, 053107 (2005).
[17] O. Jagutzki, A. Cerezo, A. Czasch, R. Dorner, M. Hattas, M. Huang, V. Mergel, U. Spillmann, K. Ullmann-Pfleger, T. Weber, H. Schmidt-Bocking, and G. Smith, IEEE Trans. Nucl. Sci. **49**, 2477 (2002).
[18] D. Rapp and D. D. Briglia, J. Chem. Phys. **43**, 1480 (1965).
[19] C. Vallance, Philos. Trans. R. Soc. Lond., A **362**, 2591 (2004).
[20] H. Adaniya, D. S. Slaughter, T. Osipov, T. Weber, and A. Belkacem, Rev. Sci. Instrum. **83**, 023106 (2012).
[21] M. Sizun and S. Goursaud, J. Chem. Phys. **71**, 4042 (1979).
[22] T. F. O'Malley and H. S. Taylor, Phys. Rev. **176**, 207 (1968).
[23] R. Azria, Y. L. Coat, G. Lefevre, and D. Simon, J. Phys. B **12**, 679 (1979).
[24] A. Moradmand, D. S. Slaughter, D. J. Haxton, T. N. Rescigno, C. W. McCurdy, T. Weber, S. Matsika, A. L. Landers, A. Belkacem, and M. Fogle, Phys. Rev. A **88**, 032703 (2013).